ACS NANO

Subscriber access provided by Universiteit Utrecht

Article

Calcium Bisphosphonates Nanoparticles with Chelator-Free Radiolabeling to Deplete Tumor-Associated Macrophages for Enhanced Cancer Radioisotope Therapy

Longlong Tian, Xuan Yi, Ziliang Dong, Jun Xu, Chao Liang, Yu Chao, Yaxing Wang, Kai Yang, and Zhuang Liu

ACS Nano, **Just Accepted Manuscript** • DOI: 10.1021/acsnano.8b06699 • Publication Date (Web): 25 Oct 2018

Downloaded from http://pubs.acs.org on October 26, 2018

Just Accepted

"Just Accepted" manuscripts have been peer-reviewed and accepted for publication. They are posted online prior to technical editing, formatting for publication and author proofing. The American Chemical Society provides "Just Accepted" as a service to the research community to expedite the dissemination of scientific material as soon as possible after acceptance. "Just Accepted" manuscripts appear in full in PDF format accompanied by an HTML abstract. "Just Accepted" manuscripts have been fully peer reviewed, but should not be considered the official version of record. They are citable by the Digital Object Identifier (DOI®). "Just Accepted" is an optional service offered to authors. Therefore, the "Just Accepted" Web site may not include all articles that will be published in the journal. After a manuscript is technically edited and formatted, it will be removed from the "Just Accepted" Web site and published as an ASAP article. Note that technical editing may introduce minor changes to the manuscript text and/or graphics which could affect content, and all legal disclaimers and ethical guidelines that apply to the journal pertain. ACS cannot be held responsible for errors or consequences arising from the use of information contained in these "Just Accepted" manuscripts.

ACS Publications

is published by the American Chemical Society. 1155 Sixteenth Street N.W., Washington, DC 20036

Published by American Chemical Society. Copyright © American Chemical Society. However, no copyright claim is made to original U.S. Government works, or works produced by employees of any Commonwealth realm Crown government in the course of their duties.

Calcium Bisphosphonates Nanoparticles with Chelator-Free Radiolabeling to Deplete Tumor-Associated Macrophages for Enhanced Cancer Radioisotope Therapy

Longlong Tian[1], Xuan Yi[2], Ziliang Dong[1], Jun Xu[1], Chao Liang [1], Yu Chao[1], Yaxing Wang[2], Kai Yang[2]*, Zhuang Liu[1]*

1. Institute of Functional Nano & Soft Materials (FUNSOM), Collaborative Innovation Center of Suzhou Nano Science and Technology, Soochow University, Suzhou, Jiangsu, 215123, China
2. State Key Laboratory of Radiation Medicine and Protection, School of Radiation Medicine and Protection & School for Radiological and Interdisciplinary Sciences (RAD-X), Collaborative Innovation Center of Radiation Medicine of Jiangsu Higher Education Institutions, Soochow University, Suzhou, Jiangsu, 215123, China

ABSTRACT: Tumor associated macrophages (TAMs) are often related with poor prognosis after radiotherapy. Depleting TAMs may thus be a promising method to improve the radio-therapeutic efficacy. Herein, we report a biocompatible & biodegradable nanoplatform based on calcium bisphosphonates (CaBP-PEG) nanoparticles for chelator-free radiolabeling chemistry, effective *in vivo* depletion of TAMs, and imaging-guided enhanced cancer radioisotope therapy (RIT). It is found that CaBP-PEG nanoparticles prepared *via* a mineralization method with polyethylene glycol (PEG) coating could be labeled with various radioisotopes upon simple mixing, including gamma-emitting ^{99m}Tc for single-photon emission computed tomography (SPECT) imaging, as well as beta-emitting ^{32}P as a therapeutic radioisotope for RIT. Upon intravenous injection, CaBP(^{99m}Tc)-PEG nanoparticles exhibit efficient tumor homing as evidenced by SPECT imaging. Owning to the function of bisphosphonates as clinical drugs to deplete TAMs, suppressed angiogenesis, normalized tumor vasculatures, enhanced intratumoral perfusion and relieved tumor hypoxia are observed after TAMs depletion induced by CaBP-PEG. Such modulated tumor microenvironment appears to be highly favorable for cancer RIT using CaBP(^{32}P)-PEG as the radio-therapeutic agent, which offers excellent synergistic therapeutic

effect in inhibiting the tumor growth. With great biocompatibility and multi-functionalities, such CaBP-PEG nanoparticles constituted by Ca^{2+} and a clinical drug would be rather attractive for clinical translation.

KEYWORDS: *bisphosphonates, biomineralized nanoparticles, chelating free radiolabeling chemistry, tumor associated macrophages, radioisotope therapy*

Radiotherapy, including external beam radiation therapy and radioisotope therapy (RIT), is a major method widely applied in current clinical cancer treatment.[1,2] The improvement of RIT depends on accurately delivering radioisotopes to tumor tissues to optimize radiation doses of tumors *versus* normal organs.[3,4] Over the recent decade, versatile nanomaterials has been developed to deliver radionuclides to tumors through the enhanced permeability and retention (EPR) effect due to the leaky tumor blood vasculature.[5-8] To minimize side effects, those nanomaterials are often designed to be biodegradable and responsive to various features within the tumor microenvironment (*e.g.* pH-sensitive, enzyme-sensitive).[9-15] Regarding the types of radio-therapeutic isotopes, as beta particles would often cause stronger damages to cancer cells compared to gamma rays because of higher linear energy transfer (LET), various types of radioisotopes, such as ^{131}I, ^{177}Lu, ^{186}Re and ^{188}Re, with both beta- and gamma decays, have been extensively applied in the clinic for RIT.[16-18] Among various therapeutic isotopes, 32-phosphorus (^{32}P) appears to be quite suitable as it is a purely beta-emitting radioisotope, and could be innately bound to DNA of cancer cells and then get trapped in tumors to effectively induce cell death.[19-22] Thus, developing biocompatible and biodegradable nanomaterials to tumor-targeted delivery of ^{32}P may be attractive for cancer RIT.

On the other hand, many features within the tumor microenvironment (TME) are known to be associated with the radio-resistance of tumor cells.[23-25] Nowadays, research into improving therapeutic outcomes of radiotherapy is focused on the role of tumor microenvironment, which may be crucial in determining the success or failure of therapy.[23] Tumor associated macrophages (TAMs), almost half weight of solid tumor mass, are considered to be a critical modulator of TME and often related with

poor prognosis.[26-30] In particular, the M2-type macrophages, the dominant type of TAMs, not only contribute to tumor growth, progress and metastasis, but also lead to immunosuppression and resistance to cancer treatments. For instance, cytokines and growth factors (*e.g.* epidermal growth factor, vascular-endothelial growth factor, matrix metalloproteinase and COX-2) overexpressed by TAMs play a key role in tumor angiogenesis, which further contributes to the abnormal tumor vasculatures and subsequent radiotherapy resistance.[31-34] Meanwhile, increasing evidences indicate that radiotherapy promotes a greater recruitment and influx of bone marrow derived TAMs into tumors.[35,36] Several strategies are under investigation for dealing with TAMs, including inhibition of macrophage recruitment, functional re-education of TAMs, as well as depletion of macrophages.[37,38] Therefore, combining TAMs targeted therapy with radiotherapy may be an attractive approach for enhanced cancer treatment.

Bisphosphonates (BP), first-line low-cost drugs to treat metabolic bone diseases, are found to show high affinity and toxicity to monocytes and their derivates, such as macrophages and osteoclasts[39]. Clophosome®, BP encapsulated in liposomes, is a commercial drug for macrophages depletion. Recent clinical trials and preclinical research results together have illustrated that the anti-tumor activity of BP is attributed to selectively target TAMs, not cancer cells.[39-41] In this work, nanoparticles mineralized from Ca^{2+} and BP by a water-in-oil reverse microemulsion method are synthesized and functionalized with polyethylene glycol (PEG).[42] CaBP-PEG nanoparticles are found to be degradable in weak acidic tumor microenvironment, favorable for TME-responsive drug release. Utilizing the multifunctional chemical property of BP, CaBP-PEG nanoparticles are labeled with ^{99m}Tc *via* coordination between phosphonate and technetium, yielding CaBP(^{99m}Tc)-PEG nanoparticles as an excellent SPECT contrast agent. Meanwhile, ^{32}P, a clinic radio-therapeutic radionuclide in the form of $^{32}PO_4^{3-}$, can also be labeled on CaBP-PEG nanoparticles *via* anion exchange, yielding CaBP(^{32}P)-PEG nanoparticles for RIT. As revealed by SPECT imaging, those BP-containing nanoparticles show efficient tumor retention after intravenous injection, and are able to effectively deplete TAMs within the tumor. Owning to the normalized tumor vasculatures, enhanced intratumoral perfusion and relieved tumor hypoxia after BP-induced TAMs depletion, CaBP(^{32}P)-PEG nanoparticles offer excellent synergistic therapeutic effect

in inhibiting the tumor growth. Considering the great biocompatibility and multi-functionalities, such CaBP-PEG nanoparticles constructed by Ca^{2+} and a clinical drug exhibit promising prospect for future clinical translation.

RESULTS AND DISCUSSION

In this work, CaBP nanoparticles were prepared by a water-in-oil reverse microemulsion method by mixing $CaCl_2$ with 1, 2-dioleoyl-sn-glycero-3-phosphate (DOPA) and BP **(Figure 1a)**. After adding excess alcohol, hydrophobic CaBP-DOPA nanoparticles were precipitated by centrifugation and then re-dispersed in chloroform by ultrasound. To transfer as-made CaBP-DOPA nanoparticles into aqueous solutions, those nanoparticles were surface modified with polyethylene glycol (PEG) through mixing with 1, 2-dihexadecanoyl-sn-glycero-3-phosphocholine (DPPC), cholesterol and 1,2-distearoyl-sn-glycero-3-phosphoethanolamine-N-(methoxy(polyethyleneglycol)-5000) ($DSPE\text{-}PEG_{5000}$) at a 4:4:2 mole ratio in chloroform.[43,44] After evaporating the solvent, CaBP-PEG nanoparticles were well dispersed in saline. Transmission electron microscopy (TEM) image **(Figure 1b)** showed that those nanoparticles were uniform in sizes. The photo of nanoparticles in PBS and medium (**Figure 1c**) illustrated that those nanoparticles exhibited high stability. Consistent to the TEM imaging results, dynamic light scatting (DLS) measurement **(Figure 1c** and **Supporting Information Figure S1)** showed the average hydrodynamic size of CaBP-PEG nanoparticles to be about 50 nm. The zeta potential of nanoparticles after PEG modification was measured to be nearly neutral at about -0.5 mV.

Considering the acid-triggered decomposition of calcium phosphate nanoparticles and the similar chemical structure between phosphate and bisphosphonate, the pH-sensitive ability of CaBP-PEG nanoparticles was tested in saline under different pH values. Under the physiological condition (pH 7.4), those nanoparticles appeared to be stable under TEM imaging without significant release of BP as measured by an Inductively Coupled Plasma Optical Emission Spectrometer (ICP-OES) (**Figure 1d&1e**). On the contrary, within acidic buffers, TEM images (**Figure 1e**) showed the corrosion of nanoparticles and ICP-OES analysis (**Figure 1d**) further confirmed the gradual release of BP during the

pH-responsive nanoparticle decomposition process. The pH-responsive property was duo to the proper pK_{a3} (about 6.6) of BP. In acidic environment, protonation process of BP would weaken the coordination between calcium ions and BP, then CaBP nanoparticles would be gradually dissolved.

Next, we studied the *in vitro* behaviors and cytotoxicity of CaBP-PEG nanoparticles. RAW264.7 murine macrophages leukemia cells were incubated with DiD dye labeled CaBP-PEG nanoparticles (**Figure 2a** and **Figure S2**). After 12 hours incubation, strong fluorescence signals in the cytoplasm of cells suggested the efficient cellular uptake of BP drugs. The cytotoxicity of CaBP-PEG nanoparticles, CaP-PEG nanoparticles (replacing BP with phosphonates as a blank control) and free BP drug to 4T1 murine breast cancer cells, CT26 murine colon carcinoma cells, 3T3 murine embryo fibroblast cells and RAW264.7 cells were measured with the standard cell viability assay (**Figure 2b-2e**). While bare CaP-PEG nanoparticles showed no appreciable toxicity to all types of cells under high concentrations, CaBP-PEG nanoparticles exhibited obviously increased cytotoxicity towards different types of cells compared to free BP, likely owing to the enhanced cellular uptake of BP in the nanoparticles formulation. Note that free BP anions are high water soluble and cannot easily pass through cell membranes.[45] The half maximal inhibitory concentrations (IC50) of CaBP-PEG nanoparticles were calculated to be 7.02 μM to RAW264.7 cells, which appeared to be much lower than that to 4T1, CT26 and 3T3 cells at 62.3 μM, 58.8 μM and 35.5 μM (**Figure 2f**), respectively, suggesting that macrophages would be much vulnerable to BP drugs compared to other cell types.

Considering the high coordination affinity of bisphosphonate with metal ions, we then speculated that CaBP-PEG nanoparticles might be labeled with $^{99m}Tc^{4+}$ (**Figure 3a**), a widely used radioactive isotope ions for single photon emission computed tomography (SPECT) imaging.[46,47] In our experiment, CaBP-PEG nanoparticles were added into the mixed solution of $Na^{99m}TcO_4$ and $NaBH_4$ (to reduce Tc^{VII} into Tc^{IV}) under weak alkaline environment. After shaking for 1 hour, free ^{99m}Tc was removed by centrifugation filtration, yielding CaBP(^{99m}Tc)-PEG nanoparticles with a radiolabeling yield at 70%. The obtained CaBP(^{99m}Tc)-PEG nanoparticles exhibited high radio-stability in PBS under 37 ^{o}C after 24 hours (**Figure 3b**). Therefore, CaBP-PEG nanoparticles could be easily labeled with radioactive isotope *via* chelator-free manner, greatly facilitating *in vivo* tracking.

Next, we used SPECT imaging to study the *in vivo* behaviors of such CaBP(^{99m}Tc)-PEG nanoparticles. Mice bearing 4T1 tumors were thus intravenously (i.v.) injected with CaBP(^{99m}Tc)-PEG nanoparticles (0.5 mCi), then imaged with SPECT imaging system. Time-dependent increase of SPECT signals (**Figure 3c**) were observed in tumor after i.v injection, suggesting the efficient tumor uptake of those PEGylated nanoparticles by the EPR effect. Significant SPECT signals were also observed in the liver of mice owing to the clearance of those nanoparticles by the reticuloendothelial system (RES).

At different time points post i.v. injection of CaBP(^{99m}Tc)-PEG nanoparticles, mouse blood samples were collected and measured the radioactive counts (**Figure 3d**). Those nanoparticles showed long blood circulation half-lives ($t_{1/2\alpha}$=0.35 h and $t_{1/2\beta}$=12.8 h). At 24 h post injection, mice were sacrificed and major organs were collected for gamma counting and biodistribution measurement (**Figure 3e**). The tumor uptake of CaBP(^{99m}Tc)-PEG nanoparticles was determined to be 5.4 % ID/g.

Considering the macrophage cytotoxicity of CaBP-PEG nanoparticles as well as their efficient tumor homing, we then wondered whether those nanoparticles could selectively deplete TAMs *in vivo*. To visually measure TAMs population changes, tumors of mice after different treatments were sliced and stained with FITC-labeled TAMs maker F4/80 antibody.[48,49] Immunofluorescence images clearly showed that TAMs positive area (green) (**Figure 4a&4b**) after PBS, CaP-PEG, free BP and CaBP-PEG treatment were 10.74%, 11.3%, 3.67% and 0.23%, respectively. Epidermal growth factor receptor (EGFR) positive area (**Figure 4a&4c**) after PBS, CaP-PEG, free BP and CaBP-PEG treatment were 67%, 64%, 52% and 35%, respectively. Consistent to *in vitro* results, while blank CaP-PEG nanoparticles and free BP treatment would not affect or only slightly decrease the population of TAMs and EGFR expression within the tumors, i.v. injected CaBP-PEG nanoparticles could lead to greatly decreased TAMs population and suppressed EGFR expression in tumors of treated mice. It is known that TAMs could be generally classified into pro-tumor M2-type and anti-tumor M1-type, among which the M2-type macrophages could be dominant within the tumor microenvironment. The percentages of $CD11^+CD206^+$ M2-type TAMs (**Figure S3**) also decreased from 0.72% to 0.13% among all collected cells, or from 4.4% to 2.2% among $CD11b^+$ monocytes, after i.v. injection of CaBP-PEG nanoparticles,

indicating the re-reduction of macrophages from immune suppressive M2-type to immune supporting M1-ype. Those results all confirmed that TAMs were selectively depleted and TAMs-stimulated angiogenesis signal would be efficiently suppressed after CaBP-PEG nanoparticles treatment.

Since intravenous administration of nanoparticles, systemic responses of mice after different treatments were conducted by testing cytokines in blood serum (**Figure 4d-4g**). After CaBP-PEG nanoparticles treatment, the level of interleukin-10 (IL-10), a pro-tumor cytokine secreted by M2-type macrophages, sharply decreased; on the contrary, the level of interleukin-12 (IL-12), an anti-tumor cytokine secreted by M1-type macrophages, greatly increased, consistently to flow cytometer measurement. In addition, the levels of tumor necrosis factor-α (TNF-α) and interferon gamma (IFN-γ), two important anti-tumor signals, coincidentally increased after TAMs depletion with CaBP-PEG nanoparticles.[50,51]

It was known that TAMs could act as barriers around tumor blood vessels, and would lead to distorted tumor blood vasculature during tumor angiogenesis. Therefore, we examined the changes of the intratumoral perfusion ability after TAMs depletion with CaBP-PEG nanoparticles by dye Evans blue assay. Mice after different treatments were i.v. injected with Evans blue. Three hours post injection, mice were scarified and tumors were collected. Photographs of tumors (**Figure 5b**) after different treatments clearly showed that intratumoral perfusion ability of Evans blue increased after CaBP-PEG nanoparticles treatment. Quantitative results (**Figure 5c**) also confirmed that tumor perfusion of mice after CaBP-PEG nanoparticles treatment almost two times than that of mice after PBS nanoparticles treatment.

Photoacoustic (PA) imaging was further conducted to directly confirm the enhanced intratumoral oxygen perfusion after CaBP-PEG nanoparticles treatment. The intratumoral oxygen perfusion was measured by vascular saturated oxygen (sO_2), which was assessed using the standard *in vivo* multispectral PA imaging with two excitation wavelengths at 750 nm and 850 nm for deoxygenated and oxygenated hemoglobin, respectively.[52] Compared to PBS and CaP-PEG treatment, sO_2 only slightly increased after free BP treatment, but greatly increased after CaBP-PEG treatment (**Figure 5d&5e**). The increased numbers of hemoglobin (**Figure S4**) also proved the enhanced tumor perfusion.

To further investigate the tumor hypoxic state after enhanced tumor oxygen perfusion, immunofluorescence staining of tumor slices was conducted. Mice bearing 4T1 tumors were sacrificed after different treatments. Hypoxia probe staining with anti-pimonidazole antibody (**Figure 5f&5g**) revealed the sharply decreased tumor hypoxia signals (green) after CaBP-PEG nanoparticles treatment, indicating that the tumor hypoxia was greatly relieved. Hypoxia inducible factor-1α (HIF-1α) overexpression (**Figure S5&S6**) was also suppressed after treatment, which would greatly help to conquer hypoxia-induced therapy-resistance. Notably, consistently to the results of down-regulation of EGFR expression, the density of tumor blood vessels (CD31 positive area) (**Figure 5g**) showed slight decrease but the numbers of dilated tumor blood vessels showed obvious increase after CaBP-PEG nanoparticles treatment (**Figure 5h**). As revealed in partially enlarged figures (**Figure 5f**), significantly ordered blood vessels were observed in CaBP-PEG group, suggesting that the enhanced intratumoral perfusion was probably attributed to anti-angiogenesis and normalized tumor vasculatures after TAMs depletion (**Figure 5a**).[53,54] All those results proved that the tumor microenvironment was effectively modulated after TAMs depletion with CaBP-PEG nanoparticles.

For cancer RIT, 32-phosphorus (^{32}P) emitting pure high energy β^--rays (1.71 MeV) could be an ideal therapeutic radionuclide. Considering the structure similarity between bisphosphonate and phosphonate, we speculated that CaBP-PEG nanoparticles might be labeled with ^{32}P in the phosphonate form *via* anion exchange (**Figure 6a**). Interesting, we found that by simply mixing CaBP-PEG nanoparticles with $Na_2H^{32}PO_4$ in weak alkaline, radioactive CaBP(^{32}P)-PEG nanoparticles could be obtain with a high radiolabeling yield (**Figure S7**) and excellent radiolabeling stability (**Figure 6b**). *In vitro* therapeutic efficacy was then determined by the cell counting kit-8 assay. CaBP(^{32}P)-PEG nanoparticles exhibited much stronger cytotoxicity than other formulations (**Figure 6c**).

Then, *in vivo* cancer therapy experiment was further carried out for 4T1 tumor bearing mice, which were randomly divided into five groups and treated with different formulations twice (**Figure 6d&6e**). Compared to PBS treated mice, treatment with non-radioactive CaBP-PEG nanoparticles and radioisotope therapy alone with either free ^{32}P and CaP(^{32}P)-PEG nanoparticles could only slightly inhibit tumor growth. Notably, treatment with CaBP(^{32}P)-PEG nanoparticles resulted in greatly delayed

tumor growth. In addition, excellent synergistic effect (combination index = 0.48) was achieved, which was owing to tumor TME modulation after TAMs depletion (**Figure S8**). Microscopy images (**Figure 6f**) of hematoxylin & eosin (H&E) stained slices from tumor of mice after different treatments also revealed that combining TAMs depletion with radioisotope therapy exhibited the heaviest cytotoxicity to tumor cells *in vivo*. The highest positive area of apoptosis maker Terminal-deoxynucleoitidyl Transferase Mediated Nick End Labeling (TUNEL) consistently proved that CaBP(^{32}P)-PEG nanoparticles caused the strongest damages to cancer cells.

To investigate the potential *in vivo* toxicity of nanomaterials and possible side effect of RIT with CaBP(^{32}P)-PEG nanoparticles, the normal organs from healthy mice as well as tumor-bearing mice after therapy were collected, sliced and then stained with H&E (**Figure S9&S10**). No significant abnormality was observed in collected organs including heart, liver, spleen, lung and kidney for mice after CaBP(^{32}P)-PEG therapy, suggesting no detectable *in vivo* toxicities under the therapy dosage. Regarding the components of those nanoparticles, calcium is an abundantly essential element, while BP is a wildly used drug in the clinic with high safety. Although free ^{32}P might exhibit marrow toxicity, the high radio-stability of CaBP(^{32}P)-PEG nanoparticles would limit the escape of free ^{32}P as evidenced by the very low bone radioactivity uptake of CaBP(^{32}P)-PEG, so as to avoid potential adverse effect. In general, those nanoparticles exhibited high biocompatibility and safety.

CONCLUSION

In this work, a biocompatible & biodegradable nanoplatform was developed for chelator-free radiolabeling chemistry, effective *in vivo* depletion of TAMs, and imaging-guided enhanced cancer radioisotope therapy (RIT). Mono-dispersed CaBP nanoparticles with uniform size were constructed with calcium ions and BP *via* a simply reverse microemulsion method. After surface PEGylation, CaBP-PEG nanoparticles with high stability in physiological condition could be gradually decomposed in acidic environment. After being labeled with a imaging radionuclide ^{99m}Tc *via* coordination, CaBP(^{99m}Tc)-PEG nanoparticles could be real-time tracked by SPECT imaging, which revealed the high tumor homing ability of those nanoparticles. Owning to the function of BP to deplete TAMs, i.v.

injection of CaBP-PEG nanoparticles would result in suppressed angiogenesis, normalized tumor vasculatures, enhanced intratumoral perfusion and relieved tumor hypoxia are observed. After being labeled with therapeutic radionuclide ^{32}P *via* anion exchange, CaBP(^{32}P)-PEG achieved excellent synergistic therapeutic effect in inhibiting the tumor growth with a combination index at 0.48.

Our nanoparticles appear to be a particularly attractive RIT platform for the following reasons: (1) Those nanoparticles are simply constituted by Ca^{2+} and a clinical drug with full biocompatibility. (2) *Via* chelator-free radiolabeling chemistry, those nanoparticles could be easily labeled either both imaging or therapeutic isotopes (^{99m}Tc and ^{32}P) upon simple mixing with high labeling yields and stabilities. It is expected that such labeling method could be extended to the labeling with other types of radioisotopes. (3) The TAM depletion function of those nanoparticles would lead to the modulated tumor microenvironment, which is found to be greatly favorable for further enhanced RIT treatment of cancer.

However, owing to the limited access to radioisotopes in our radio-lab until now, in this study, only cation $^{99m}Tc^{4+}$ and anion $^{32}PO_4^{3-}$ were labeled on CaBP-PEG nanoparticles for imaging and therapy, respectively. Although no significant toxicity was observed in our experiments at our treatment dose, one note is that ^{32}P with a half-life of 14.3 days may not be the ideal type of radioisotope for RIT application upon systemic administration. Local administration of those nanoparticles into tumors may be an alternative approach for tumor treatment to avoid potential systemic toxicity. Moreover, we also expect that our CaBP-PEG nanoparticles could be easily labeled with other types of therapeutic radioisotopes with shorter half-lives (*e.g.* ^{90}Y, ^{177}Lu ^{188}Re) *via* the same chelate-free labeling method following that used for ^{99m}Tc labeling, to enable more effective cancer RIT. Nevertheless, our work presents a biocompatible RIT nano-platform capable of chelate-free radiolabeling and effective modulation of tumor microenvironment, promising for cancer RIT with enhanced efficacy.

MATERIALS AND METHODS

Synthesis and Surface Modification of Nanoparticles. Hydrophobic DOPA-coated CaBP nanoparticles were prepared using a water-in-oil micro-emulsion method. 30 mL water-in-oil solution was prepared by mixing 4.35 mL CO-520 (as surfactant), 2.25 mL Triton-100 (as surfactant), 1.5 mL

1-hextrol and 21.9 mL cyclohexane together (CO-520/Triton X-100/hextol/cyclohexane = 10.5/7.5/5/77, v/v/v/v) and separated into two halves. 300 μL 25 mM BP solution in 0.5 M Tris buffer (pH 10) and 400 μL 20 mg/mL DOPA in chloroform were added in 15 ml of the water-in-oil solution as P phase. 300 μL 500 mM $CaCl_2$ in 0.5 M Tris buffer (pH 10) was added in 15 ml of the water-in-oil solution as Ca phase. The clear P phase was slowly dropped in the Ca phase with a micro-injection pump under stirring. After stirring overnight, equivalent volume of ethanol was added to precipitate the DOPA-coated nanoparticles. Then the obtained nanoparticles were washed with ethanol for three times to remove impurities.

The DOPA-coated CaBP nanoparticles were re-dispersed in chloroform and treated with ultrasonic for 30 mins to acquire well mono-dispersed nanoparticles. Then DPPC, cholesterol and DSPE-PEG (5k) were added in the solution. After violently stirring overnight, the chloroform was removed through rotary evaporation. Finally, the surface modified CaBP-PEG nanoparticles were re-dispersed in saline solution. 1 mg/mL $CaCl_2$ could be added to stabilize nanoparticles in saline for long-term storage. CaP-PEG nanoparticles were synthesized as control through replacing BP with phosphate (Na_3PO_4).

For fluorescence labeling of nanoparticles, 10 μL 5mg/mL DiD dye in methanol was added in 1 mL CaBP-PEG (2mg/mL) solution. After stirring overnight and ultrafiltration, DiD-labeled CaBP-PEG nanoparticles were obtained.

Characterization. The DOPA-coated CaBP nanoparticles were re-dispersed in cyclohexane and characterized by transmission electron microscopy. The hydrodynamic size of CaBP-PEG nanoparticles was determined by a Zetasizer Nano-ZS (Malvern Instruments, UK). To test the pH responsive property, CaBP-PEG nanoparticles were encapsulated in dialysis bag (MWCO = 1000) and put in saline solution under different pH values (7.4, 6.5 and 5.5). After stirring for different times, the concentration of released phosphorus was measured by ICP-OES.

Cellular experiment. 4T1, CT26 cells, 3T3 cells and RAW264.7 cells were cultured under recommended conditions. For *in vitro* toxicity assay, four types of cells seeded into 96-well plates were

incubated with free BP, CaP-PEG or CaBP-PEG nanoparticles at different concentrations for 24 h. The methyl thiazolyl tetrazolium (MTT) assay was then conducted to determine cytotoxicity of the three formulations to four cell lines.

Radiolabeling of ^{99m}Tc. One mCi $Na^{99m}TcO_4$ (purchased from Shanghai GMS Pharmaceutical Co., Ltd) and 100 μL 10 mg/mL $NaBH_4$ (as the reductant) were added into the CaBP-PEG solution. After shaking for 1 hour, the free technetium and excess reductant were remove by centrifugation filtration and washed with saline until no detachable radioactivity in the filtration solution, yielding CaBP(^{99m}Tc)-PEG nanoparticles.

Animal Model. Female Balb/c mice (purchased from Nanjing Peng Sheng Biological Technology Co., Ltd) were used under standard protocols approved by Soochow University Laboratory Animal Center. To build subcutaneous tumor model, 1×10^6 4T1 cells in 50 μL of PBS were subcutaneously injected into the back of each mouse. Ten days after injection, tumor volumes of mice reached about 100 mm^3.

SPECT Imaging and *in vivo* Behaviors of Nanoparticles. Balb/c mouse bearing 4T1 tumors (~200 mm^3) was i.v. injected with CaBP(^{99m}Tc)-PEG nanoparticles (0.5 mCi) and imaged with a small animal SPECT (MILabs, Utrecht, the Netherlands) imaging system at 2, 6 and 12 h post injection. For nanoparticles pharmacokinetics, at different time points post injection of CaBP(^{99m}Tc)-PEG, ~20 μL of blood was drawn from right orbital venous plexus. The radioactivities in blood samples were measured by a gamma counter (LB211, Berthold Technologies Gmbh & Co.KG). At 24 h post injection, the mice were sacrificed. All major organs and tumor were collected and weighed. Radioactivities of samples were measured.

Assays about TAMs Depletion and Tumor Microenvironment Modulation. A total of 12 Balb/c mice with 4T1 tumors (about 100 mm^3) were divided in three groups and treated with PBS, CaP-PEG

nanoparticles or CaBP-PEG nanoparticles (200 μL, 1 mg/mL). The treatment was repeated 4 days later. After waiting for another 3 days, tumors were collected and cut into two halves for flow cytometry assay and immunofluorescence staining. For flow cytometer analysis, tumor cells were collected after homogenization and stained with FITC-anti-CD206 and PE-anti-CD11b antibodies. For immunofluorescence imaging, tumors were fixed with OCT glue for sections. Then slices were stained with DAPI, FITC-anti-F4/80 or anti-EGFR (abcam52894) antibody. Moreover, the immunofluorescence imaging of tumor hypoxia was conducted by using either the pimonidazole probe, or anti-HIF-1α antibody, following previously reported protocol.[52] Immunofluorescence images were captured by Olympus confocal fluorescence microscopy. For cytokine measurement, mice sera were collected for ELISA assays to test the levels of IL-10, IL-12, TNF-α and IFN-γ.

Evaluation of Intratumoral Perfusion. A total of 12 4T1 tumor-bearing mice (about 100 mm^3) were treated with PBS, CaP-PEG nanoparticles or CaBP-PEG nanoparticles (200 μL, 1 mg/mL) for twice at day 0 and day 4. Tumor oxygen perfusion was directly measured with Photoacoustic Imaging System (Vevo LAZR) at 0 and 24 h post the first injection. Three days after the second treatment, all mice were i.v. injected with 5% Evans blue. Three hours after treatment, mice were scarified and tumors were collected and weighed. Evans blue was extracted from the tumor tissues with dimethyl formamide for three days, and quantitated with a UV-vis spectrophotometer at 620 nm.

Radiolabeling of 32-Phosphorus and *in vivo* Therapy. $Na_2H^{32}PO_4$ (purchased from China Isotope and Radiation Corporation) solution was added into CaBP-PEG or CaP-PEG nanoparticles solution under shaking at 60 °C overnight. Free radioisotopes were removed through centrifugation filtration. For the *in vitro* cytotoxicity assay, 4T1 cells incubated with different concentrations of CaBP-PEG, free ^{32}P, CaP(^{32}P)-PEG or CaBP(^{32}P)-PEG for 72 h. Then MTT assay was conducted to test the cytotoxicity of different formulation. For *in vivo* therapy, 25 Balb/c mice bearing 4T1 tumors with sizes about 100 mm^3 were randomly divided in five groups treated with PBS, CaBP-PEG, free ^{32}P, CaP(^{32}P)-PEG, or CaBP(^{32}P)-PEG (100 μCi of ^{32}P and/or 200 μg of BP). Four days later, the treatment was repeated.

Tumor volumes were measure with a caliper. The combination index (CI) = AB/(A×B).[52] In this equation, AB is the tumor volume ratio of the CaBP(^{32}P)-PEG group to the PBS group, while A or B is the tumor volume ratio of CaP(^{32}P)-PEG group or CaBP-PEG group to the PBS group, respectively.

ASSOCIATED CONTENT

Supporting Information Available online: confocal imaging data; flow cytometry histograms; PA hemoglobin statistics; HIF-1α immunofluorescence staining; HIF-1α expression statistics; radiolabeling yields; H&E staining micrographs.

The authors declare no competing financial interest.

AUTHOR INFORMATION

Corresponding Authors

*E-mail: kyang@suda.edu.cn.

*E-mail: zliu@suda.edu.cn.

ORCID

Kai Yang: 0000-0002-6670-1024

Zhuang Liu: 0000-0002-1629-1039

ACKNOWLEDGEMENTS

This work was partially supported by the National Research Programs from Ministry of Science and Technology (MOST) of China (2016YFA0201200), the National Natural Science Foundation of China (51525203, 31822022, 81471716, 51761145041), a Jiangsu Natural Science Fund for Outstanding Youth Science Foundation (BK20180094), Collaborative Innovation Center of Suzhou Nano Science and Technology, a ‘111’ program from the Ministry of Education (MOE) of China, and a Project Funded by the Priority Academic Program Development (PAPD) of Jiangsu Higher Education Institutions.

REFERENCES

(1) D'Amico, A. V.; Whittington, R.; Malkowicz, S. B.; Cote, K.; Loffredo, M.; Schultz, D.; Chen, M. H.; Tomaszewski, J. E.; Renshaw, A. A.; Wein, A.; Richie, J. P. Biochemical Outcome after Radical Prostatectomy or External Beam Radiation Therapy for Patients with Clinically Localized Prostate Carcinoma in the Prostate Specific Antigen Era. *Cancer* **2002**, *95*, 281-286.

(2) Mcewan, A. J. Radioisotope Therapy and Clinical Trial Design: the Need for Consensus and Innovation. *J. Nucl. Med.* **2002**, *43*, 87-88.

(3) Pagel, J. M.; Hedin, N.; Subbiah, K.; Meyer, D.; Mallet, R.; Axworthy, D.; Theodore, L. J.; Wilbur, D. S.; Matthews, D. C.; Press, O. W. Comparison of Anti-CD20 and Anti-CD45 Antibodies for Conventional and Pretargeted Radioimmunotherapy of B-Cell Lymphomas. Blood **2003**, *101*, 2340-2348.

(4) Carlsson, J.; Forssell, A. E.; Hietala, S. O.; Stigbrand, T.; Tennvall, J. Tumour Therapy with Radionuclides: Assessment of Progress and Problems. *Radiother. Oncol.* **2003**, *66*, 107-117.

(5) Prabhakar, U.; Maeda, H.; Jain, R. K.; Sevick-Muraca, E. M.; Zamboni, W.; Farokhzad, O. C.; Barry, S. T.; Gabizon, A.; Grodzinski, P.; Blakey, D. C. Challenges and Key Considerations of the Enhanced Permeability and Retention Effect for Nanomedicine Drug Delivery in Oncology. *Cancer Res.* **2013**, *73*, 2412-2417.

(6) Peng, C. L.; Shih, Y. H.; Lee, P. C.; Hsieh, M. H.; Luo, T. Y.; Shieh, M. J. Multimodal Image-Guided Photothermal Therapy Mediated by 188Re-Labeled Micelles Containing a Cyanine-Type Photosensitizer. *ACS Nano* **2011**, *5*, 5594-5607.

(7) Yi, X.; Yang, K.; Liang, C.; Zhong, X.; Ning, P.; Song, G.; Wang, D.; Ge, C.; Chen, C.; Chai, Z.; Liu, Z. Imaging-Guided Combined Photothermal and Radiotherapy to Treat Subcutaneous and Metastatic Tumors Using Iodine-131-Doped Copper Sulfide Nanoparticles. *Adv. Funct. Mater.* **2015**, *25*, 4689-4699.

(8) Zhong, X.; Yang, K.; Dong, Z.; Yi, X.; Wang, Y.; Ge, C.; Zhao, Y.; Liu, Z. Polydopamine as a Biocompatible Multifunctional Nanocarrier for Combined Radioisotope Therapy and Chemotherapy of Cancer. *Adv. Funct. Mater.* **2016**, *25*, 7327-7336.

(9) Shen, S.; Li, H. J.; Chen, K. G.; Wang, Y. C.; Yang, X. Z.; Lian, Z. X.; Du, J. Z.; Wang, J. Spatial Targeting of Tumor-Associated Macrophages and Tumor Cells with a pH-Sensitive Cluster Nanocarrier for Cancer Chemoimmunotherapy. *Nano Lett.* **2017**, *17*, 3822-3829.

(10) Deng, Z.; Zhen, Z.; Hu, X.; Wu, S.; Xu, Z.; Chu, P. K. Hollow Chitosan-Silica Nanospheres as pH-Sensitive Targeted Delivery Carriers in Breast Cancer Therapy. *Biomaterials* **2011**, *32*, 4976-4986.

(11) Han, H.; Valdepérez, D.; Qiao, J.; Yang, B.; Li, Z.; Wu, Y.; Pelaz, B.; Parak, W. J.; Jian, J. Dual Enzymatic Reaction-Assisted Gemcitabine Delivery Systems for Programmed Pancreatic Cancer Therapy. *ACS Nano* **2017**, *11*, 1281-1291.

(12) Qiu, M.; Wang, D.; Liang, W.; Liu, L.; Zhang, Y.; Chen, X.; Sang, D. K.; Xing, C.; Li, Z.; Dong, B.; Xing, F.; Fan, D.; Bao, S.; Zhang, H.; Cao, Y. Novel Concept of the Smart NIR-Light-Controlled Drug Release of Black Phosphorus Nanostructure for Cancer Therapy. *Proc. Natl. Acad. Sci. U. S. A.* **2018**, *115,* 501-506.

(13) Wang, J.; Yang, G.; Guo, X.; Tang, Z.; Zhong, Z.; Zhou, S. Redox-Responsive Polyanhydride Micelles for Cancer Therapy. *Biomaterials* **2014**, *35*, 3080-3090.

(14) Qiu, M.; Ren, W. X.; Jeong, T.; Won, M.; Park, G. Y.; Sang, D. K.; Liu, L. P.; Zhang, H.; Kim, J. S. Omnipotent Phosphorene: a Next-Generation, Two-Dimensional Nanoplatform for Multidisciplinary Biomedical Applications. *Chem. Soc. Rev.* **2018**, *47,* 5588-5601.

(15) Chen, Q.; Wang, X.; Wang, C.; Feng, L.; Li, Y.; Liu, Z. Drug-Induced Self-Assembly of Modified Albumins as Nano-Theranostics for Tumor-Targeted Combination Therapy. *ACS Nano* **2015**, *9*, 5223-5233.

(16) Miller, R. C.; Marino, S. A.; Brenner, D. J.; Martin, S. G.; Richards, M.; Randers-Pehrson, G.; Hall, E. J. The Biological Effectiveness of Radon-Progeny Alpha Particles. II. Oncogenic Transformation as a Function of Linear Energy Transfer. *Radiat. Res.* **1995**, *142*, 54-60.

(17) Kassis, A. I.; Adelstein, S. J. Radiobiologic Principles in Radionuclide Therapy. *J. Nucl. Med.* **2005**, *46*, 4-12.

(18) Hoefnagel, C. A. Radionuclide Cancer Therapy. *Ann. Nucl. Med.* **1998**, *12*, 61-70.

(19) Zimmer, A. M.; Silverstein, E. A.; Holmes, R. A. Assay of 32P-Sodium Phosphate Using a Commercial Dose Calibrator. *J. Nucl. Med.* **1976**, *17*, 404-405.

(20) Reddy, M. V.; Gupta, R. C.; Randerath, E.; Randerath, K. 32P-Postlabeling Test for Covalent DNA Binding of Chemicals *in Vivo*: Application to a Variety of Aromatic Carcinogens and Methylating Agents. *Carcinogenesis* **1984**, *5*, 231-243.

(21) Gest, H. The Early History of 32P as a Radioactive Tracer in Biochemical Research: A Personal Memoir. *Biochem. Mol. Biol. Ed.* **2005**, *33*, 159-164.

(22) Pratt, D.; Stent, G. S.; Harriman, P. D. Stabilization to 32P Decay and Onset of DNA Replication of T4 Bacteriophage. *J. Mol. Biol.* **1961**, *3*, 409-424.

(23) Barker, H. E.; Paget, J. T.; Khan, A. A.; Harrington, K. J. The Tumour Microenvironment after Radiotherapy: Mechanisms of Resistance and Recurrence. *Nat. Rev. Cancer* **2015**, *15*, 409-425.

(24) Zhang, J.; Shen, Y.; Dong, J. Research Progress of Relationship Between Tumor Microenvironment and Radioresistance. *Cancer Res. Clin.* **2015**, *27*, 61-63.

(25) Barcelloshoff, M. H.; Cordes, N. Resistance to Radio and Chemotherapy and the Tumour Microenvironment. *Int. J. Radiat. Biol.* **2009**, *85*, 920-922.

(26) Chen, Z.; Feng, X.; Herting, C. J.; Garcia, V. A.; Nie, K.; Pong, W. W.; Rasmussen, R.; Dwivedi, B.; Seby, S.; Wolf, S. A.; Gutmann, D. H.; Hambardzumyan, D. Cellular and Molecular Identity of Tumor-Associated Macrophages in Glioblastoma. *Cancer Res.* **2017**, *77*, 2266-2278.

(27) Zhang, J.; Yan, Y.; Yang, Y.; Wang, L.; Li, M.; Wang, J.; Liu, X.; Duan, X.; Wang, J. High Infiltration of Tumor-Associated Macrophages Influences Poor Prognosis in Human Gastric Cancer Patients, Associates with the Phenomenon of EMT. *Medicine* **2016**, *95*, 2636.

(28) Zhang, W.; Wang, L.; Zhou, D.; Cui, Q.; Zhao, D.; Wu, Y. Expression of Tumor-Associated Macrophages and Vascular Endothelial Growth Factor Correlates with Poor Prognosis of Peripheral T-Cell Lymphoma, not Otherwise Specified. *Leukemia Lymphoma* **2011**, *52*, 46-52.

(29) Daurkin, I.; Eruslanov, E.; Stoffs, T.; Perrin, G. Q.; Algood, C.; Gilbert, S. M.; Rosser, C. J.; Su, L. M.; Vieweg, J.; Kusmartsev, S. Tumor-Associated Macrophages Mediate Immunosuppression in the Renal Cancer Microenvironment by Activating the 15-Lipoxygenase-2 Pathway. *Cancer Res.* **2011**, *71*, 6400-6409.

(30) Chanmee, T.; Ontong, P.; Konno, K.; Itano, N. Tumor-Associated Macrophages as Major Players in the Tumor Microenvironment. *Cancers* **2014**, *6*, 1670-1690.

(31) Batchelor, T. T.; Sorensen, A. G.; Di, T. E.; Zhang, W. T.; Duda, D. G.; Cohen, K. S.; Kozak, K. R.; Cahill, D. P.; Chen, P. J.; Zhu, M. AZD2171, a Pan-VEGF Receptor Tyrosine Kinase Inhibitor, Normalizes Tumor Vasculature and Alleviates Edema in Glioblastoma Patients. *Cancer Cell* **2007**, *11*, 83-95.

(32) Lewis, C. E.; Pollard, J. W. Distinct Role of Macrophages in Different Tumor Microenvironments. *Cancer Res.* **2006**, *66,* 605-612.

(33) Valković, T.; Dobrila, F.; Melato, M.; Sasso, F.; Rizzardi, C.; Jonjić, N. Correlation Between Vascular Endothelial Growth Factor, Angiogenesis, and Tumor-Associated Macrophages in Invasive Ductal Breast Carcinoma. *Virchows Arch.* **2002**, *440*, 583-588.

(34) Raposo, T. P.; Pires, I.; Carvalho, M. I.; Prada, J.; Argyle, D. J.; Queiroga, F. L. Tumour-Associated Macrophages are Associated with Vascular Endothelial Growth Factor Expression in Canine Mammary Tumours. *Vet. Comp. Oncol.* **2015**, *13*, 464-474.

(35) Russell, J. S.; Brown, J. M. The Irradiated Tumor Microenvironment: Role of Tumor-Associated Macrophages in Vascular Recovery. *Front. Physiol.* **2013**, *4*, 157.

(36) Miller, M. A.; Chandra, R.; Cuccarese, M. F.; Pfirschke, C.; Engblom, C.; Stapleton, S.; Adhikary, U.; Kohler, R. H.; Mohan, J. F.; Pittet, M. J.; Weissleder, R. Radiation Therapy Primes Tumors for Nanotherapeutic Delivery *via* Macrophage-Mediated Vascular Bursts. *Sci. Transl. Med.* **2017**, *9*, 0225.

(37) Ngambenjawong, C.; Gustafson, H. H.; Pun, S. H. Progress in Tumor-Associated Macrophage (TAM)-Targeted Therapeutics. *Adv. Drug Deliver. Rev.* **2017**, *114,* 206-221.

(38) Mantovani, A.; Marchesi, F.; Malesci, A.; Laghi, L.; Allavena, P. Tumour-Associated Macrophages as Treatment Targets in Oncology. *Nat. Rev. Clin. Oncol.* **2017**, *14*, 399-416.

(39) Rogers, T. L.; Ingunn, H. Tumour Macrophages as Potential Targets of Bisphosphonates. *J. Transl. Med.* **2011**, *9*, 177.

(40) Junankar, S.; Shay, G.; Jurczyluk, J.; Ali, N.; Down, J.; Pocock, N.; Parker, A.; Nguyen, A.; Sun, S.; Kashemirov, B. Real-time Intravital Imaging Establishes Tumor-Associated Macrophages as the Extraskeletal Target of Bisphosphonate Action in Cancer. *Cancer Discov.* **2015**, *5*, 35-42.

(41) Kimura, N. Y.; Nakao, S.; Basaki, Y.; Ueda, S.; Takamori, S.; Shirouzu, K.; Kuwano, M.; Ono, M. The Role of Macrophages in Tumor Growth and Angiogenesis by Lung Cancer Cells-Inhibition by Bisphosphonate-Liposomes. *Cancer Res.* **2006**, *66*, 394-395.

(42) Au, K. M.; Satterlee, A.; Min, Y.; Tian, X.; Kim, Y. S.; Caster, J. M.; Zhang, L.; Zhang, T.; Huang, L.; Wang, A. Z. Folate-Targeted pH-Responsive Calcium Zoledronate Nanoscale Metal-Organic Frameworks: Turning a Bone Antiresorptive Agent into an Anticancer Therapeutic. *Biomaterials* **2016**, *82*, 178-193.

(43) Dong, Z.; Feng, L.; Zhu, W.; Sun, X.; Min, G.; He, Z.; Yu, C.; Zhuang, L. CaCO3 Nanoparticles as an Ultra-Sensitive Tumor-pH-Responsive Nanoplatform Enabling Real-Time Drug Release Monitoring and Cancer Combination Therapy. *Biomaterials* **2016**, *110*, 60-70.

(44) Li, J.; Chen, Y. C.; Tseng, Y. C.; Mozumdar, S.; Huang, L. Biodegradable Calcium Phosphate Nanoparticle with Lipid Coating for Systemic siRNA Delivery. *J. Control. Release* **2010**, *142*, 416-421.

(45) Zhang, Y.; Cao, R.; Yin, F.; Hudock, M. P.; Guo, R. T.; Krysiak, K.; Mukherjee, S.; Gao, Y. G.; Robinson, H.; Song, Y.; No, J. H.; Bergan, K.; Leon, A.; Cass, L.; Goddard, A.; Chang, T. K.; Lin, F. Y.; Van Beek, E.; Papapoulos, S.; Wang, A. H.; *et al*. Lipophilic Bisphosphonates as Dual Farnesyl/Geranylgeranyl Diphosphate Synthase Inhibitors: An X-ray and NMR Investigation. *J. Am. Chem. Soc.* **2009**, *131*, 5153-5262.

(46) Ogawa, K.; Mukai, T.; Inoue, Y.; Ono, M.; Saji, H. Development of a Novel 99mTc-Chelate-Conjugated Bisphosphonate with High Affinity for Bone as a Bone Scintigraphic Agent. *J. Nucl. Med.* **2006**, *47*, 2042-2047.

(47) Tji, T. G.; Vink, H. A.; Gelsema, W. J.; Ligny, C. L. D. Determination of the Oxidation State of Tc in 99Tc(Sn)EHDP, 99mTc(Sn)EHDP, 99Tc(Sn)MDP and 99mTc(Sn)MDP Complexes. Characterization of Tc(III)-, Tc(IV)- and Tc(V)EHDP Complexes. *Appl. Radiat. Isotopes* **1990**, *41*, 17-28.

(48) Kalra, A.; Klinz, S.; Paz, N.; Kim, J.; Chalishazar, M.; Drummond, D.; Kirpotin, D.; Moyo, V.; Niyikiza, C.; Fitzgerald, J. Abstract 5696: Evaluating Determinants for Enhanced Activity of MM-398/PEP02; a Novel Nanotherapeutic

Encapsulation of Irinotecan (CPT-11). *Cancer Res.* **2012**, *72*, 5696-5696.

(49) Muthana, M.; Rodrigues, S.; Chen, Y. Y.; Welford, A.; Hughes, R.; Tazzyman, S.; Essand, M.; Morrow, F.; Lewis, C. E. Macrophage Delivery of an Oncolytic Virus Abolishes Tumor Regrowth and Metastasis after Chemotherapy or Irradiation. *Cancer Res.* **2013**, *73*, 490-495.

(50) Pan, B.; Farrugia, A. N.; To, L. B.; Findlay, D. M.; Green, J.; Lynch, K.; Zannettino, A. C. The Nitrogen-Containing Bisphosphonate, Zoledronic Acid, Influences RANKL Expression in Human Osteoblast-Like Cells by Activating TNF-Alpha Converting Enzyme (TACE). *J. Bone Miner. Res.* **2004**, *19*, 147-154.

(51) Tanaka, Y.; Iwasaki, M.; Murata-Hirai, K.; Matsumoto, K.; Hayashi, K.; Okamura, H.; Sugie, T.; Minato, N.; Morita, C. T.; Toi, M. Anti-Tumor Activity and Immunotherapeutic Potential of a Bisphosphonate Prodrug. *Sci. Rep.* **2017**, *7*, 5987.

(52) Tian, L.; Chen, Q.; Yi, X.; Wang, G.; Chen, J.; Ning, P.; Yang, K.; Liu, Z. Radionuclide I-131 Labeled Albumin-Paclitaxel Nanoparticles for Synergistic Combined Chemo-Radioisotope Therapy of Cancer. *Theranostics* **2017**, *7*, 614-623.

(53) Zeisberger, S. M.; Odermatt, B.; Marty, C.; Zehnderfjällman, A. H. M.; Ballmerhofer, K.; Schwendener, R. A. Clodronate-Liposome-Mediated Depletion of Tumour-Associated Macrophages: a New and Highly Effective Antiangiogenic Therapy Approach. *Brit. J. Cancer* **2006**, *95*, 272-281.

(54) Piaggio, F.; Kondylis, V.; Pastorino, F.; Di, P. D.; Perri, P.; Cossu, I.; Schorn, F.; Marinaccio, C.; Murgia, D.; Daga, A.; Raggi, F.; Loi, M.; Emionite, L.; Ognio, E.; Pasparakis, M.; Ribatti, D.; Ponzoni, M.; Brignole, C. A Novel Liposomal Clodronate Depletes Tumor-Associated Macrophages in Primary and Metastatic Melanoma: Anti-Angiogenic and Anti-Tumor Effects. *J. Control. Release* **2016**, *223*, 165-177.

TOC Figure

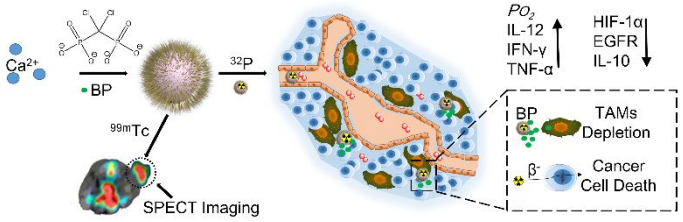

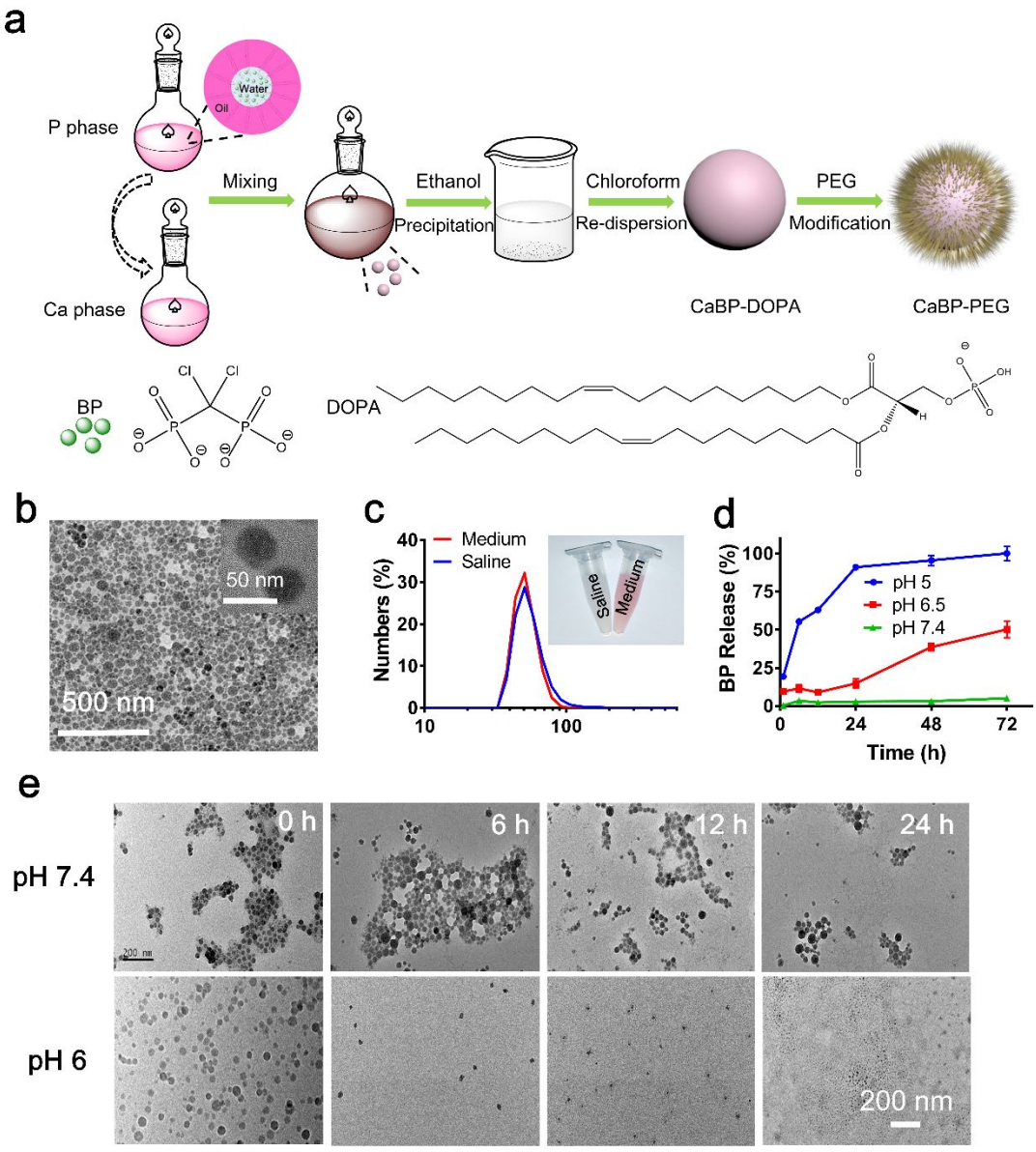

Figure 1. Preparation and characterization of nanomaterials. (a) A schematic illustration to show the preparation of CaBP nanoparticles. (b) A TEM image of CaBP nanoparticles. (c) Dynamic light scattering data and photo of CaBP-PEG nanoparticles in PBS and cell culture medium buffer. (d) Release of BP from CaBP-PEG nanoparticles under different pH values. (e) TEM images of CaBP-PEG nanoparticles in physiological (pH 7.4) and acidic (pH 6) buffers after incubation for different periods of time.

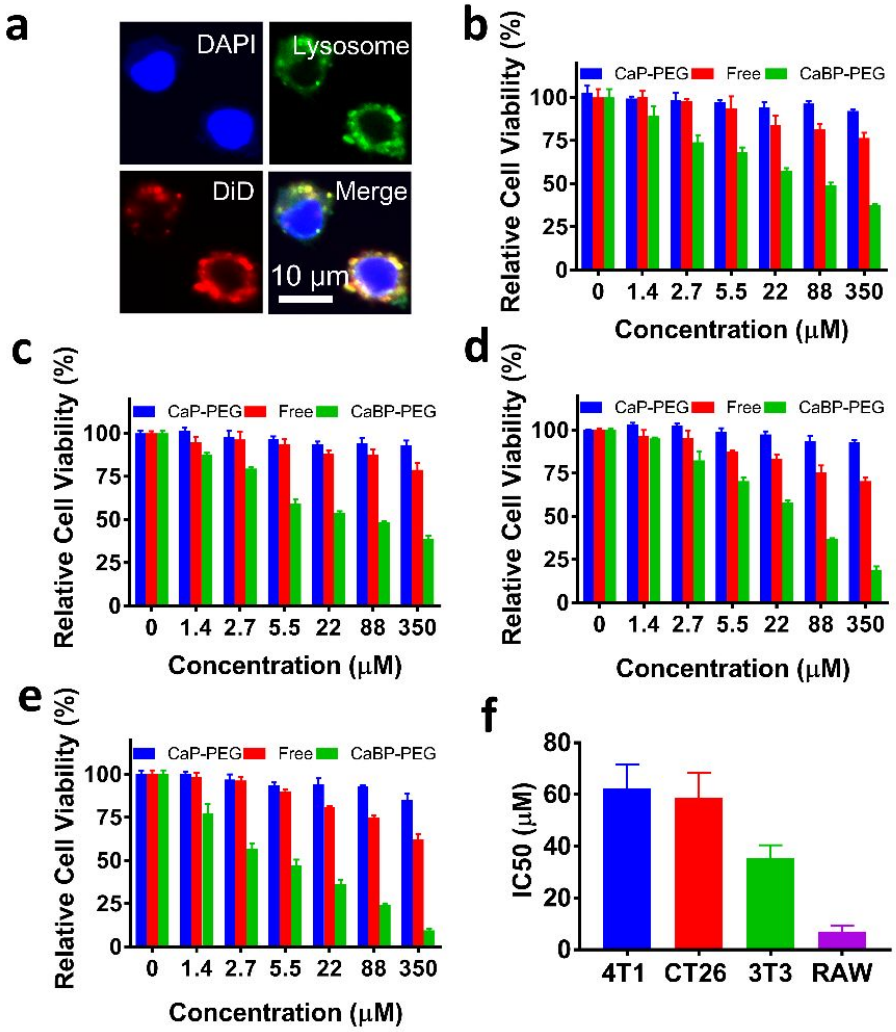

Figure 2. *In vitro* behaviors of nanoparticles. (a) Confocal fluorescence images of RAW cells after incubation with DiD labeled CaBP-PEG nanoparticles for 12 h. Cell nuclei and lysosomes were labeled by DAPI and lyso-tracker®, respectively. Cytotoxicity of CaP-PEG nanoparticles, free BP and CaBP-PEG nanoparticles to 4T1 (b), CT26 (c), 3T3 (d) and RAW264.7 (e) cells at different bisphosphonate or phosphonate concentrations. (f) Half maximal inhibitory (IC50) concentrations of CaBP-PEG nanoparticles were 62.3 μM, 58.8 μM, 35.5 μM and 7.02 μM, for 4T1, CT26, 3T3, and RAW264.7 cells, respectively.

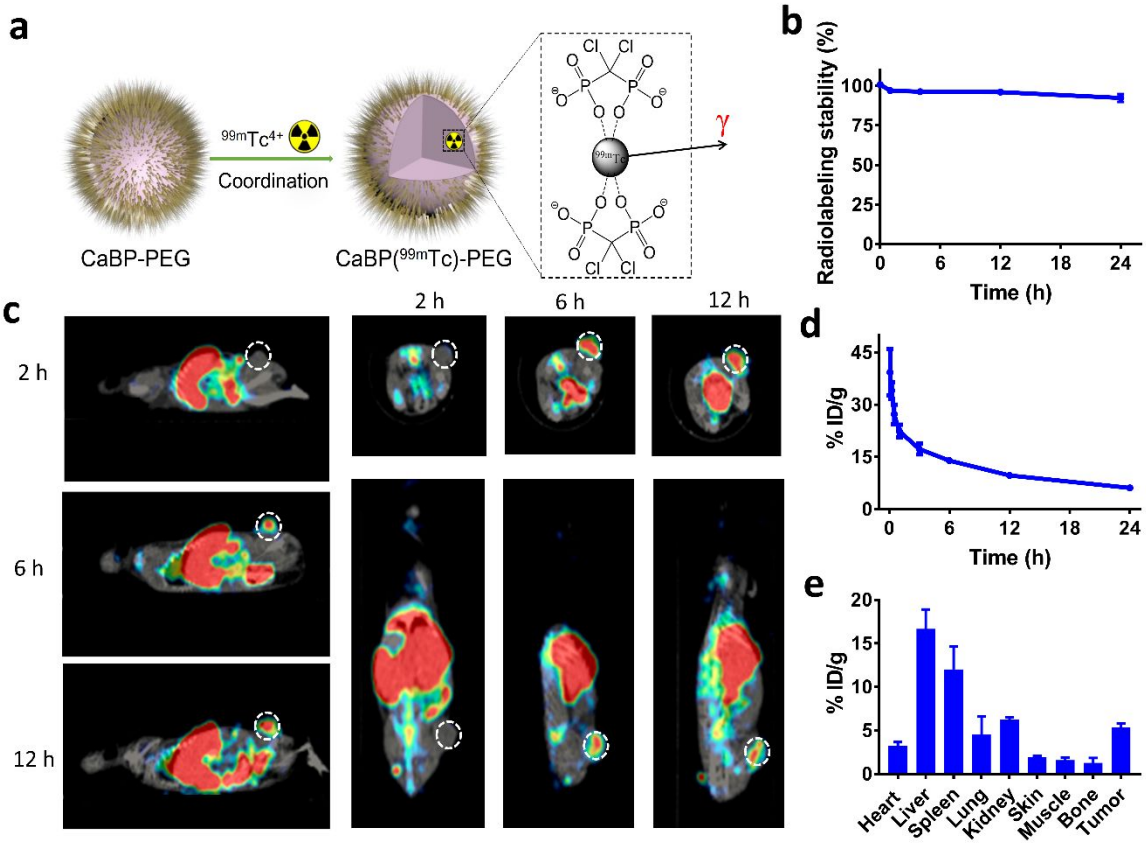

Figure 3. *In vivo* behaviors of nanoparticles. (a) A scheme illustration of ^{99m}Tc radiolabeling of CaBP-PEG nanoparticles for tracing *in vivo* fate of nanoparticles. (b) The radiolabeling stability of ^{99m}Tc labeled CaBP-PEG nanoparticles. (c) SPECT images of mice at 2, 6 and 12 h after intravenous injection of CaBP(^{99m}Tc)-PEG nanoparticles. Tumors of mice were highlighted by the dotted circles. (d) The blood circulation profiles of CaBP(^{99m}Tc)-PEG nanoparticles. (e) The biodistribution of CaBP(^{99m}Tc)-PEG nanoparticles measured at 24 h post injection.

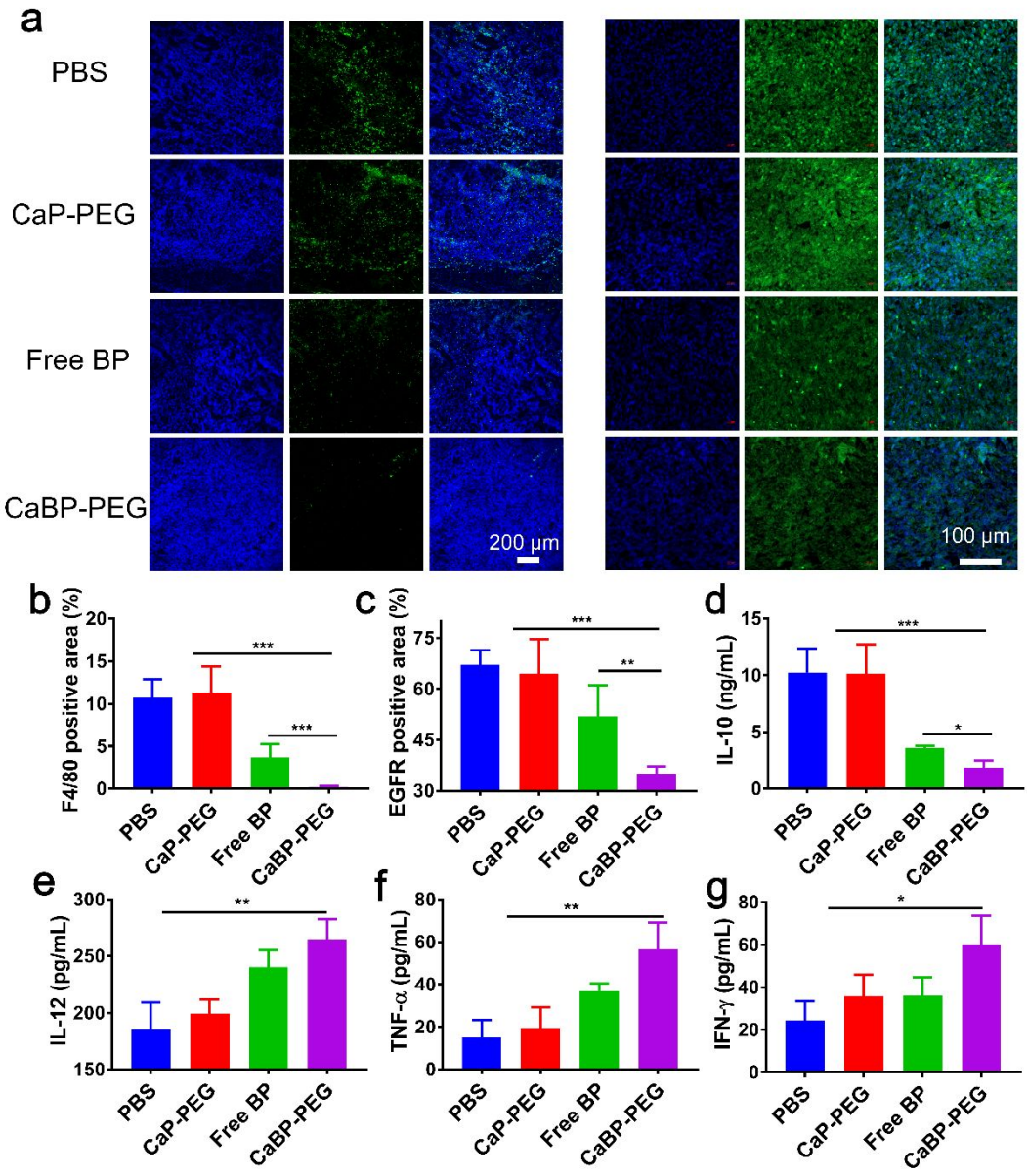

Figure 4. Selective depletion of TAMs with CaBP-PEG nanoparticles treatment. (a) TAMs (left) and TAMs-stimulated EGFR expression (right). Immunofluorescence images of tumor slices stained with DAPI (blue), anti-F4/80 (green, left) or anti-EGFR (green, right) antibody. (b-c) Statistic data of F4/80 and EGFR positive area percentages in tumors after different treatments. F4/80 and EGFR positive signals sharply decreased after CaBP-PEG nanoparticles treatment. (d-g) The levels of IL-10, IL-12, TNF-α and IFN-γ in sera of mice after different treatments. All the above assays were conducted at 3 days post second i.v. injection of various agents indicated. P value in (b-g) determined with t-test. *$p < 0.05$, **$p < 0.01$, ***$p < 0.001$.

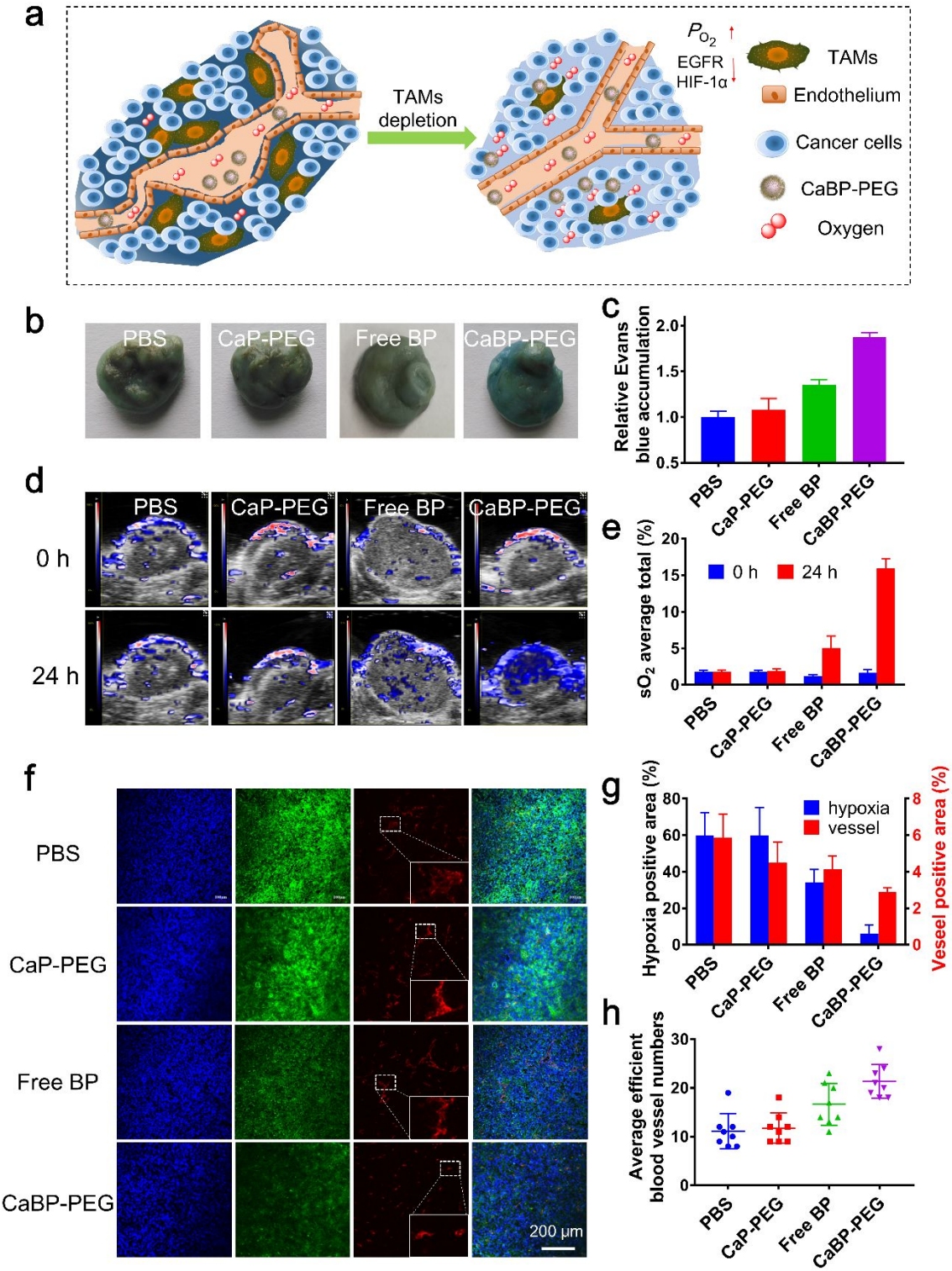

Figure 5. *In vivo* modulation of tumor microenvironment after CaBP-PEG nanoparticles treatment. (a) A scheme showing the normalized tumor vasculature, enhanced perfusion and relieved tumor hypoxia after TAMs depletion. (b) Photographs of tumors after extraction of Evans blue. The deep blue in tumors of mice after CaBP-PEG nanoparticles treatment indicted the enhanced intratumoral perfusion. (c) Relative

Evans blue accumulation in tumors measured with a UV-vis spectrophotometer at 620 nm after DMF extraction. (d) Photoacoustic imaging showing tumor saturated O_2 levels of mice after i.v. injection of PBS, CaP-PEG, free BP or CaBP-PEG nanoparticles. (e) Tumor average total sO_2 from (d). (f) Representative immunofluorescence images of tumor slices collected from mice treated with PBS, CaP-PEG, free BP or CaBP-PEG nanoparticles. The cell nuclei, blood vessels, and hypoxia areas were stained with DAPI (blue), anti-CD31 antibody (red), and anti-pimonidazole antibody (green), respectively. (g) Percentages of hypoxia-positive and CD31-positive areas from (f). (h) Numbers of dilated tumor blood vessels from (f). More than 10 images were analyzed for each sample to obtain the statistic information.

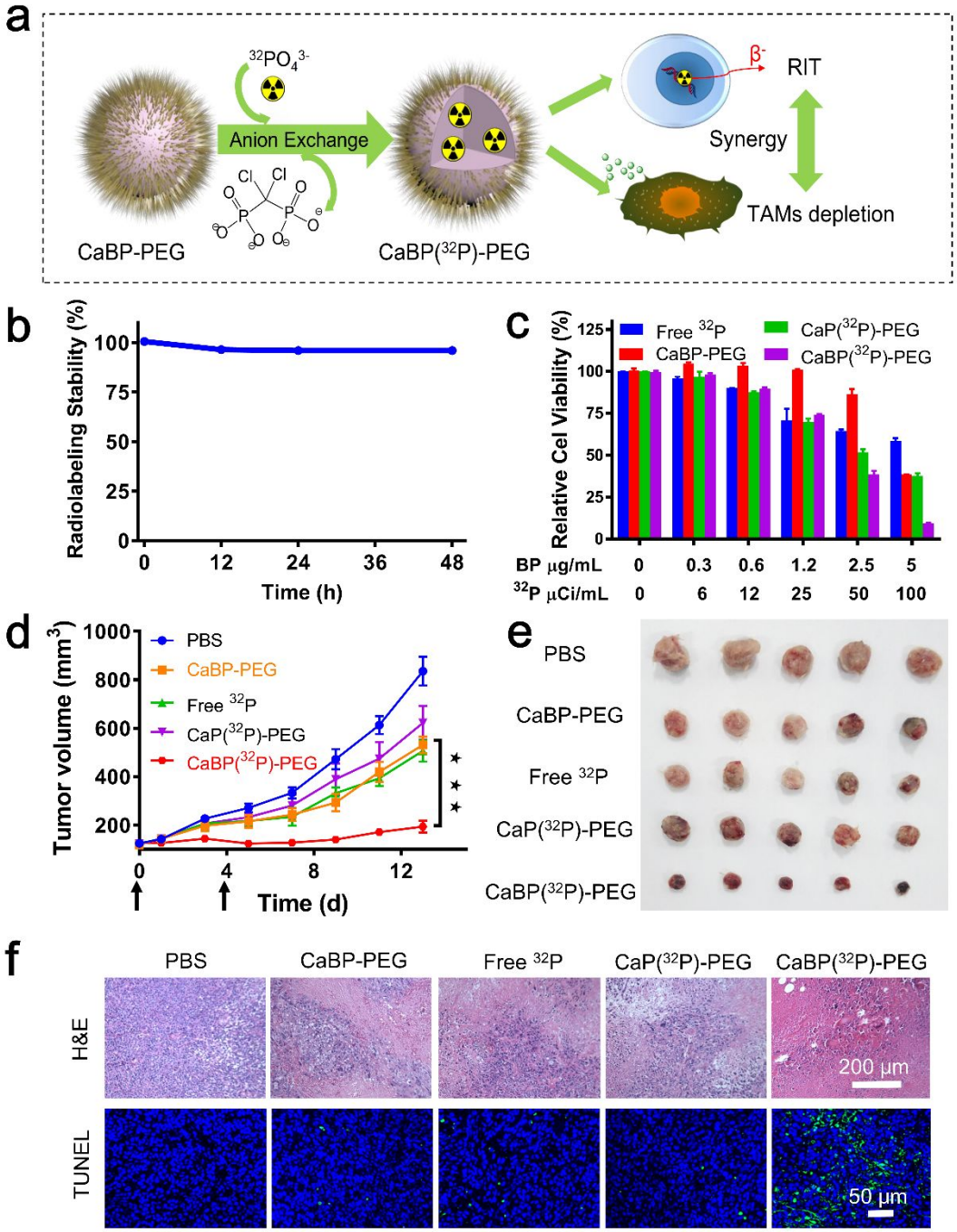

Figure 6 *In vitro* and *in vivo* therapeutic efficiency of CaBP(^{32}P)-PEG nanoparticles. (a) A scheme illustration of CaBP(^{32}P)-PEG nanoparticles for synergistic combination RIT with TAMs depletion. (b) Radiolabeling stability of CaBP(^{32}P)-PEG nanoparticles. (c) The relative cell viabilities of 4T1 cells incubated with of free ^{32}P, CaP(^{32}P)-PEG, CaBP-PEG or CaBP(^{32}P)-PEG nanoparticles for 72 h. (d) Tumor volume curves of mice with various treatments. Doses for each injection: 100 μCi of ^{32}P, 200 μg of BP. The mice were treated twice at day 0 and 4 (black arrows). (e) Photographs of tumors collected at the fourteenth day after first treatment. (f) Images of H&E and TUNEL stained tumor slices after

various treatments. P values in (d) were calculated with t-test (***$p < 0.001$).